Atmos. Chem. Phys. Discuss., 14, 12727–12769, 2014
www.atmos-chem-phys-discuss.net/14/12727/2014/
doi:10.5194/acpd-14-12727-2014

Atmospheric Chemistry and Physics
Discussions
Open Access

Analysis of elevated spring-time levels of Peroxy Acetyl Nitrate (PAN) at the High Alpine research sites Jungfraujoch and Zugspitze

S. Pandey Deolal[1], S. Henne[2], L. Ries[3], S. Gilge[4], U. Weers[1], M. Steinbacher[2], J. Staehelin[1], and T. Peter[1]

[1]Institute for Atmospheric and Climate Science, Swiss Federal Institute of Technology (ETH), Zurich, Switzerland
[2]Laboratory for Air Pollution/Environmental Technology, Swiss Federal Laboratories for Materials Science and Technology (Empa), Duebendorf, Switzerland
[3]Air Monitoring Network, Environment Agency Germany (UBA), Platform Zugspitze Schneefernerhaus (ZSF) of GAW-Global Station Zugspitze/Hohenpeissenberg, Germany
[4]Hohenpeissenberg Meteorological Observatory, German Meteorological Service (DWD), Hohenpeissenberg, Germany

Received: 3 April 2014 – Accepted: 29 April 2014 – Published: 20 May 2014

Correspondence to: J. Staehelin (johannes.staehelin@env.ethz.ch)

Published by Copernicus Publications on behalf of the European Geosciences Union.

Abstract

Largest atmospheric peroxy acetyl nitrate (PAN) mole fractions at remote surface sites in the Northern Hemisphere are commonly observed during the months April and May. Different formation mechanisms for this seasonal maximum have previously been suggested: hemispheric-scale production from precursors accumulated during the winter months, increased spring-time transport from up-wind continents, increased regional-scale production in the atmospheric boundary layer from recent emissions. The two high Alpine research sites Jungfraujoch (Switzerland) and Zugspitze (Germany) exhibit a distinct and consistent spring-time PAN maximum, too. Since these sites intermittently sample air masses of free tropospheric and boundary layer origin, they are ideally suited to identify the above mentioned PAN formation processes and attribute local observations to these. Here we present a detailed analysis of PAN observations and meteorological conditions during May 2008 when PAN levels were especially elevated at both sites. Highest PAN concentrations were connected with anti-cyclonic conditions, which persisted in May 2008 for about 10 days with north easterly advection towards the sites. A backward dispersion model analysis showed that elevated PAN concentrations were caused by the combination of favourable photochemical production conditions and large precursor concentrations in the European atmospheric boundary layer. The results suggest that the largest PAN values in spring 2008 at both sites were attributable to regional-scale photochemical production of PAN in the (relatively cold) planetary boundary layer from European precursors whereas the contribution of inter-continental transport or free tropospheric build-up was of smaller importance for these sites.

1 Introduction

Peroxy Acetyl Nitrate (PAN) is a reactive nitrogen species, which can serve as an indicator of photochemical processing in the troposphere and is, as such, better suited than ozone (O_3) since there are no direct natural sources of PAN, e.g. no export from the stratosphere as in the case of O_3, and background concentrations are close to negligible. On the other hand PAN decomposes rapidly at higher temperatures and monitoring of PAN mixing ratios is much more sophisticated than that of ozone. PAN plays an important role in the chemistry of the troposphere because it acts as relatively long lived reservoir for nitrogen oxides (NO_x) that, at cold temperatures, can be transported over long distances and, hence, contribute to inter-continental transport of O_3 precursors (Penkett and Brice, 1986; Nielsen et al., 1981; Rappenglück et al., 2010; Schrimpf et al., 1998; Tsalkani et al., 1991). It is well known that PAN exhibits a strong seasonal cycle, peaking in spring in the northern hemispheric remote atmosphere (Moxim et al., 1996). These PAN spring maxima were often explained in the following way: the mixing ratios of long-lived NMVOC (non-methane volatile organic compounds) accumulate in the free troposphere (FT) over the winter season due to less efficient photo-degradation (Penkett et al., 1993); in early spring photochemistry becomes active and the accumulated NMVOC in the northern FT foster the build-up of PAN and O_3 leading to the observed maximum in both species in the background troposphere (Penkett and Brice, 1986; Monks, 2000; Zanis et al., 2003, 2007; Fenneteaux et al., 1999). The seasonal pattern indicated by these studies leads to the perception that the spring maximum is not directly influenced by recent emissions into the planetary boundary layer (PBL) but is a background air phenomenon. In contrast, there are other studies explaining PAN spring maxima in terms of long range transport or special meteorological situations (Fischer et al., 2010; Ridley et al., 1998) or a combination of both free tropospheric and PBL air masses (Bottenheim et al., 1994).

PAN measurements reported during the period 1987–1988 from three Swiss sites (suburban station, Dübendorf, 431 m a.s.l.; forest site, Laegeren, 685 m a.s.l.; Alpine valley site, Davos, 1630 m a.s.l.) showed significant seasonal variation in PAN with elevated monthly mean values in spring for all the stations, suggesting that maximum PAN concentrations were associated with anti-cyclonic weather types and low wind speeds (Wunderli and Gehrig, 1991). Previous PAN observations at the Swiss high

Alpine site Jungfraujoch (JFJ) revealed maximum PAN levels > 1 ppb in spring-summer season and attributed the maxima to thermally-induced transport from the PBL (Zellweger et al., 2003). These and additional measurements of PAN at JFJ were recently presented in an analysis using hemispheric scale backward trajectories, which showed that the spring maximum of PAN is most pronounced for air masses that had recent contact with the European PBL (Pandey Deolal et al., 2013). In contrast to previous findings, their results suggest that, to a large part, the spring PAN maximum originates from recent precursor emissions and effective PAN production in the PBL followed by further export to the FT at JFJ.

Based on the above discussion there are three hypotheses for the origin of the PAN spring maximum at remote and high altitude sites in Europe:

1. increased background concentrations: build-up of precursor during winter in the Northern Hemisphere, active photochemistry producing high PAN concentrations in spring in the free troposphere;
2. boundary layer influence and meteorologically favourable situations: transport from the boundary layer, e.g. by convective transport and/or accumulation in anticyclonic air flow;
3. inter-continental transport: increased background mixing ratios (for e.g. ozone) from inter-continental transport during spring as shown by recent studies (Cooper et al., 2010; Fiore et al., 2009).

This paper aims to elucidate which of these hypothesis is responsible for the spring PAN maximum in the FT over the Alps. To this end we present PAN observations from two high Alpine sites, Jungfraujoch (Switzerland) and Zugspitze (Germany), in the context of transport regimes during the month of May 2008, when particularly large PAN mole fractions were reported at these sites. In addition, observations from nearby elevated rural sites (Rigi and Chaumont (Switzerland) and Hohenpeissenberg (Germany)), which are more representative for the day-time PBL, are used to further interpret the processes responsible for the build-up of large PAN mole fractions.

2 Site characterization and measurements

The main sites used in this study (Jungfraujoch and Zugspitze, but also the PBL site Hohenpeissenberg) are so called “global stations” of the Global Atmosphere Watch (GAW) programme of the World Meteorological Organization (WMO), while the two additional Swiss sites are regional (Rigi) and contributing (Chaumont) stations to GAW. For all sites detailed measurement and site information can be found in the GAW station information system (GAWSIS, http://gaw.empa.ch/gawsis). The Swiss sites are also part of the Swiss National Air Pollution Monitoring Network (NABEL), which is operated by the Swiss Federal Laboratories for Materials Science and Technology (Empa) in collaboration with the Swiss Federal Office for Environment (FOEN) (Empa and FOEN, 2013). The measurements at Zugspitze are supported by the Federal Environment Agency (UBA) and regular monitoring of meteorological parameters and atmospheric radioactivity is performed by the German Weather Service (DWD). Continuous measurements of relevant gaseous species and aerosols are performed at all sites. An overview of all the sites is provided in Table 1 and their locations are shown in Fig. 1.

2.1 Site characterization

2.1.1 High Alpine sites (Jungfraujoch and Zugspitze)

The observatory at Jungfraujoch (Sphinx observatory, 3580 m a.s.l.) is situated between the Mönch and the Jungfrau mountains in the Bernese Alps of Switzerland. The site is intermittently influenced by the lower FT and European PBL air and, therefore, provides the opportunity to characterize air masses with very different origin and air mass history. Air arriving from the north is often influenced by surface contact over the Swiss plateau before reaching JFJ, while air masses arriving from the south are often advected from the Po Valley crossing the inner Alpine region (Parker et al., 2009; Zellweger et al., 2003).

The Zugspitze Schneefernerhaus (ZSF, 2670 m a.s.l.) observatory is situated in southern Germany at the northern rim of the Alps. Therefore, it is suitable for the detection of air masses advected from the north (Kaiser et al., 2007). The measurement station is situated on the southern slope of Zugspitze between the summit and a skiing area. Normally, Zugspitze receives free tropospheric air but, similar to JFJ, the site is frequently exposed to boundary layer air in summer time due to thermally-induced flow systems (Gantner et al., 2003; Reiter et al., 1987). In comparison to JFJ, a stronger influence of surface emissions on the trace gas observations at ZSF was deduced and the site was placed into a different category ("weakly influenced") as JFJ ("mostly remote") in a study categorising remote air quality sampling sites in Europe (Henne et al., 2010). The altitude difference between the two sites is about ~ 900 m, while the horizontal distance is around ~ 250 km.

2.1.2 PBL sites – Hohenpeissenberg (HPB), Rigi (RIG) and Chaumont (CHA)

The Hohenpeissenberg observatory (HPB) is another GAW site located in Germany, about 40 km north of Zugspitze in a hilly area dominated by agriculture and forests. The site is predominantly situated in the day-time PBL and night-time residual layer as it is located on top of a small mountain (985 m a.s.l.) and about 300 m above the surrounding area.

The station Rigi (RIG) (1031 m a.s.l.) is situated on the northern slope of the Rigi mountain, in an elevated rural environment 600 m above Lake Lucerne. The site is surrounded by grass-land and forest areas and small cities such as Zug and Lucerne are approximately 12 km away from the site and at considerably lower elevation. Rigi is located about 65 km north-east of JFJ. The Chaumont observatory (CHA) (1136 m a.s.l.) is located about 700 m above Lake Neuchatel. The area is dominated by meadows and pastures. The city of Neuchatel is situated about 5 km south of the station, but well below at the lake shore. The station is located about 90 km north-west of JFJ. Both Swiss sites can be expected to be within the day-time PBL during the spring and summer months, while they are more decoupled from lowland influences during night and winter.

2.2 Trace gas measurements

2.2.1 Jungfraujoch

The air was sampled from the main inlet dedicated for trace gas observations, which has a total length of about 3 m, with 2 m on the roof top and 1 m inside the laboratory. The inlet consists of stainless steel tubing with an inner diameter of 90 mm and is constantly heated to 10 °C. The air flow rate was 50 $m^3 hr^{-1}$. The PAN instrument was directly connected to the main inlet using PFA tubing. Since PAN measurements are sensitive to temperature, the instrument was placed close to the main inlet avoiding further heating to laboratory temperatures.

PAN measurements were performed at JFJ using commercial gas chromatograph (GC) analyzer and a calibration unit provided by Meteorologie Consult GmbH (Metcon). The technique is based on chromatographic separation with subsequent detection and quantification by an electron capture detector (ECD). For more details see Pandey Deolal et al. (2013). Other trace gases such as total reactive nitrogen species (NO_y), nitrogen oxides (NO_x), CO and O_3 are routinely monitored as part of the NABEL monitoring network (Empa and FOEN, 2013). NO_y, NO_x and NO measurements at JFJ were performed using high sensitive analyzers (ECO physics CLD 89p) based on a chemiluminescence technique. More details are presented in Pandey Deolal et al. (2012). CO measurements were performed using a commercially available instrument (APMA-370, Horiba) based on non-dispersive infrared absorption (NDIR). Ozone was measured using a commercially available monitor (Thermo Environmental Instruments, Model 49C, UV absorption). The measurements of CO and O_3 are described in more detail in Zellweger et al. (2003, 2009).

2.2.2 Zugspitze

The air was sampled with the UBA steel inlet used for measuring reactive gases. The total length of the inlet is 3.5 m with 2.25 m on the roof top and 1.25 m inside the laboratory. A borosilicate glass tube was placed inside the steel inlet with inner glass diameter of 80 mm. The inlet is constantly heated to +6 °C.

PAN measurements at ZSF were performed using the same technique and instrument as described for JFJ measurements. NO_y, NO measurements were performed using CRANOX, ECO physics (2x CLD 770 AL pptv) containing a gold converter and two reaction chambers. The gold converter is heated to 300 °C with 2 % CO (99.997 %, Air Liquide). NO_x was measured as NO after the photolytic conversion by the photolytic converter (PLC 760 MH) instrument. The converter efficiency of the gold converter mainly ranged between 95–98 % and conversion efficiency of PLC ranged from 61 to 82 %. The detection limit for NO_y and NO channel was 50 pptv. The time resolution of these measurements was 145 s. Calibrations were performed twice a week. The typical drift of the calibration span signal for NO during four days was 1.1–1.4 %

2.2.3 Hohenpeissenberg

PAN measurements at this site were started in the late 1990's and continued till present, using the same equipment as for JFJ and ZSF. Additionally the PAN measurements at HPB have been quality tested by at a blind inter-comparison experiment at NCAR, Boulder, CO (Tyndall et al., 2005). Long term analysis of CO, nitrogen dioxide (NO_2) and O_3 time series was reported by (Gilge et al., 2010) where these measurements were also compared with other Alpine sites JFJ, ZSF and Hoher Sonnblick.

Title Page
Abstract | Introduction
Conclusions | References
Tables | Figures
◀ | ▶
◀ | ▶
Back | Close
Full Screen / Esc
Printer-friendly Version
Interactive Discussion

2.2.4 Rigi and Chaumont

A variety of trace gases and aerosol parameters (such as NO_2, O_3, particulate matter and volatile organic compounds (VOC)) as well as meteorology are routinely performed at Rigi and Chaumont (Empa and FOEN, 2013).

3 Transport analysis

3.1 Backward dispersion simulations

The Lagrangian Particle Dispersion Model (LPDM) FLEXPART (Version 8.1) (Stohl et al., 2005) was used to calculate source receptor relationships (SRR) for May 2008 measurements for the two high Alpine sites. For each 3 hourly interval 50 000 particles were released at each receptor site (JFJ and ZSF) and traced back in time for 10 days considering the mean flow, turbulent PBL flow and deep convection. The model was driven by European Centre for Medium Range Weather Forecast (ECMWF) operational analyses (00:00, 06:00, 12:00, 18:00 UTC) and forecasts (03:00, 09:00, 15:00, 21:00 UTC) with 91 vertical level and a horizontal resolution of 1° by 1° for the global domain and 0.2° by 0.2° for a nested domain covering the Alpine area (4° W–16° E, 39–51° N). Compared to the aforementioned study by Pandey Deolal (2013), which drew its conclusions from single trajectory simulations, the present transport simulations are better suited to quantitatively capture the influence of the European PBL on the observations at the high Alpine sites since FLEXPART explicitly simulates turbulent and convective mixing that cannot be represented in single-trajectory models.

Release heights of 3000 m and 2500 m were chosen for JFJ and ZSF, respectively. This is significantly lower than the true altitudes of the observatories and takes into account the limited horizontal resolution of the model, by which the Alpine topography is not well represented, requiring a release height somewhere between the station's real altitude and the model ground (Brunner et al., 2012; Keller et al., 2012).

The simulated SRRs allow directly linking a mass release at a source grid cell with a mass mixing ratio at the receptor (Seibert and Frank, 2004). SRRs are given in units s m^3 kg^{-1} and are also referred to as footprints and emission sensitivities. SRRs were generated on a regular grid with 0.1° by 0.1° covering western Europe (Fig. 4) and a secondary grid with 0.5° by 0.5° horizontal resolution covering the larger North Atlantic region (see Fig. S1 in the Supplement). The vertical resolution of both grids was restricted to 10 levels up to 15 km above model ground, the lowest of these with a 100 m thickness above ground.

3.2 Footprint clustering

In order to see the effects of different flow regimes on PAN concentrations, simulated SRRs were classified into different flow regimes applying clustering methods to the transport simulations but not to the observed trace species. A straightforward approach would be to treat the SRR in every cell of the output grid as an individual time series in the cluster analysis. However, in that case the number of variables would become too large to be handled efficiently and arbitrary results might be produced due to the inclusion of grid cells with very small SRRs. Therefore, we reduced the number of grid cells by aggregating cells with small average (May 2008) emission sensitivities to larger grid cells. Starting from grid cells with 0.1° resolution we allowed aggregation to grid cells with up to 3.2° horizontal resolution. Only SRRs in the lowest output level were considered. This grid reduction is similar to the method that was used in regional inversion studies where it is beneficial to reduce the dimension of the inversion problem (Vollmer et al., 2009; Keller et al., 2011). We iteratively varied the SRR threshold for grid aggregation to obtain approximately 100 grid cells (cluster variables) for the calculation of the dissimilarity matrix required by the clustering algorithm. Only the European domain was considered for the clustering, which will focus the separation of flow situations more onto the continental scale transport to the sites and to a lesser degree onto the inter-continental transport. However, as will be discussed in Sect. 4, the model results for May 2008 did not suggest any significant inter-continental transport from North-America during this period and, hence, the focus on the European domain is justified in this case. Since the time series of aggregated SSRs were not normally or log-normally distributed, we chose an alternative distance measure to obtain the dissimilarity matrix, **D** with elements d_{ij}. Instead of the usually applied Euclidean distance we calculated absolute distances between the ranks of the SRRs within the time series

$$d_{ij} = \sum_{l:1,N} \left| \mathrm{rank}(\mathrm{SRR}_l)_i - \mathrm{rank}(\mathrm{SRR}_l)_j \right|, \tag{1}$$

where index l runs over all times N and i and j refer to the individual grid cells. Here rank stands for the sample rank of values in a vector. If ties (same values within vector) existed these were given an average rank. Once the dissimilarity matrix is formed, the clustering was done using k-medoids clustering (Kaufman and Rousseeuw, 1990). The number of clusters was obtained using the silhouette technique (Kaufman and Rousseeuw, 1990) by choosing the number of clusters (in the range 2 to 20) for which the average silhouette widths became maximal. The technique described here is similar to the one presented by Hirdman et al. (2010) for Arctic sites and essentially the same as applied by (Sturm et al., 2013) to FLEXPART simulations for JFJ for a period of three years.

The clustering was applied to the time series of the aggregated emission sensitivities for both high Alpine sites separately. For JFJ the maximal silhouette width was at 4 clusters, while for ZSF the situation was more complicated. Here the overall maximum silhouette width was obtained for 18 clusters, which gave a much too fine separation of the transport situations. Other local maxima were at 3 and 5 clusters. The clustering with 5 clusters was more similar to the one obtained for JFJ. Hence, 5 clusters were retained for ZSF.

For each cluster, average surface SRRs were calculated by summation over all cluster members and division by the number of cluster members N_c

$$\mathrm{RTC}^{c}_{i,j,k} = \frac{\sum\limits_{l \in C} \mathrm{SRR}_{i,j,k,l}}{N_c}, \tag{2}$$

where i, j, k represent the spatial indices and l the temporal. The index c identifies the cluster number.

4 Results and discussion

4.1 Seasonal cycle of PAN

PAN measurements from different sites are shown in Fig. 2. At JFJ, PAN measurements were performed during campaigns in 2008 for the spring–summer (May and August) and autumn (September and October) months. The monthly mean mixing ratios of PAN for both JFJ and ZSF are presented in Fig. 2 (left panel). These measurements indicate a strong seasonal cycle in the PAN with peaking mole fractions in late spring (April or May) and minima in the autumn and winter months. Prior to recent measurements, PAN observations at JFJ from April 1997–May 1998 (black solid line) also revealed a similar annual cycle (Zellweger et al., 2000). PAN measurements at JFJ performed during campaigns between February 2005 and August 2006 (black crosses) by Balzani Lööv et al. (2008) indicated background mole fractions < 0.2 ppb in April and May however, spring mean mole fractions were found significantly lower than all other reported measurements. Campaign measurements during February/March 2003 at JFJ showed mean concentrations of 0.142 ppb (Whalley et al., 2004), which is in agreement with the observations from other years. Figure 2 (right panel) shows the PAN measurements at the PBL sites including HPB and the Swiss sites Dübendorf (sub-urban), Lageren (rural forest) and Davos (Alpine valley, 1630 m a.s.l.) taken from Wunderli and Gehrig (1991).

All these measurements in the PBL, also including the Alpine valley site, clearly show the same seasonal behaviour and are in line with previous observations of spring PAN maxima at northern hemispheric mid-latitudes (Penkett and Brice, 1986; Monks, 2000; Zanis et al., 2007, 2003; Fenneteaux et al., 1999). The only exception showing a summer maximum are the measurements of HPB in 2003 which is most probably caused by the special conditions of the European heat wave in summer 2003 (e.g. Ordonez et al., 2010).

Since high Alpine sites intermittently receive FT and PBL air, it should be possible to attribute high PAN observations to either the FT or PBL, if the air mass contributions can be clarified. The only spring month for which relatively complete PAN time series were available from both high Alpine sites was May 2008. In addition, JFJ experienced large average PAN mixing ratios during this month, while PAN at ZSF was comparable to other years. Therefore, May 2008 was selected for a more detailed analysis as the variability at the sites can help identifying the potential origin of air masses and meteorological processes involved.

4.2 Observations in May 2008

4.2.1 Meteorological conditions

The entire month was characterized by an alternation between rather stagnant high and low pressure systems over Europe. A low pressure system with its centre over the North Sea and the UK prevailed from the beginning of the month until 5 May. From 6–11 May, distinct high pressure conditions developed over southern Scandinavia extending south- and eastward towards Central and Eastern Europe. This resulted in high irradiation and cloud free conditions in Central and parts of Eastern Europe and this period was considered as blocking anti-cyclonic conditions (Hamburger et al., 2011). Towards the end of this period pressure gradients weakened and the deep convection potential increased resulting in local thunderstorms over the Alps and Jura mountains on 12 May. From 13–17 May the situation over Central and Western Europe was dominated by a low pressure system moving from the Gulf of Biscay towards northern Germany. The Alpine area was influenced by the frontal systems embedded in this lower pressure system. As a result, irradiation (cloud cover) was reduced (enhanced) south and west of the Alps. A south foehn situation developed on 15 and 16 May with precipitation on the southern side of the Swiss Alps. From 17 to 31 May, low pressure conditions persisted over Central Europe leading to a succession of frontal passages.

4.2.2 Observations at JFJ and ZSF

The time series of trace gas observations at JFJ and ZSF are shown in Fig. 3 for May 2008. The PAN mixing ratios at JFJ were especially high during the period 6–15 May reaching a 3 hourly maximum of 1.2 ppb. PAN was elevated during the same period at ZSF as well, but did not exceed 1 ppb.

In addition to PAN, other trace species such as NO_y, CO and O_3 showed increased mixing ratios during this period at both sites as well, while NO_x mixing ratios remained comparably low (Fig. 3). After 15 May PAN levels dropped at both sites and remained between 0.1 and 0.5 ppb for the rest of the month.

In general PAN levels were lower (factor 0.7) and NO_x and NO_y levels were greater (factor 2.9 and 1.4, respectively) at ZSF as compared to JFJ. The monthly average contribution of PAN to total NO_y was about 59 % and 26 % for JFJ and ZSF, respectively. Part of this difference may be related to the temperature difference between the sites and the connected difference in thermal decomposition of PAN. The average temperature of +1.5 °C and −5.0 °C at ZSF and JFJ, respectively, during the high PAN episode can be translated to average PAN lifetimes with respect to thermal decomposition of $\tau =\sim 1$ day and $\tau =\sim 5$ days for ZSF and JFJ, respectively. Temperature differences were reduced between 20 May and 24 May but strongly increased after. However, overall a weak negative correlation (Pearson correlation coefficient: $R = -0.17$) was observed between PAN differences and temperature differences between the sites, suggesting that processes other than thermal decomposition are more important for the observed differences.

O_3 levels were generally greater at JFJ as compared with ZSF and specific humidity was generally smaller, most likely due to the higher altitude of the JFJ observatory. An exception to this observation is the period 3 May to 6 May, when the lowest O_3 mole fractions occured during May 2008 at JFJ. At the same time CO levels were decreased and humidity increased. Unfortunately, PAN measurements are missing for 4 May to 6 May at JFJ and, when looking at the PAN decrease on 3 May, it can only be assumed that PAN levels were low as well (supported by the fact that NO_y mixing ratios remained low, too). Trace gas mole fractions at ZSF did not show any special event during the same period. Furthermore, an episode of high NO_x mole fractions was observed at ZSF on 21 and 22 May, which is also reflected in relatively low O_3 mole fractions at the same time and site. Another pronounced event was encountered at JFJ on 23 May when O_3 levels increased to a monthly maximum and CO and specific humidity strongly decreased at the same time. This is indicative for stratospheric influence that was not encountered at ZSF at this time.

Ozone was strongly correlated with PAN in May 2008 with Pearson correlation coefficient $R = 0.70$ and $R = 0.80$ for JFJ and ZSF respectively, indicating photochemically well processed air masses in which significant amounts of PAN and ozone were formed simultaneously.

4.2.3 Footprint cluster analysis

To further analyse the conditions that led to the observed variability in PAN observations and especially the period of elevated PAN the trace gas time series were split into different categories according to the transport clustering described above (footprint clustering). Since the clustering is based on transport history of the observed air masses only, it is thought to shed light on the main question of this article as to which extent the observed spring maximum in PAN can be related to free tropospheric, hemispheric background scale production of PAN from accumulated precursors or regional scale production from recent emissions.

As described above, the clustering resulted in 4 and 5 clusters for JFJ and ZSF respectively. The results of the clustering in terms of temporal attribution can be seen in Fig. 3, in which the time series were coloured according to the transport cluster. It can directly be seen that the individual clustering at the sites resulted in relatively similar temporal cluster attributions at both sites. When considering that clusters 4 and 5 at ZSF could actually be joined to be comparable to cluster 4 at JFJ, the detected transport regimes match between the sites in 91 % of all cases. Keeping in mind that the clustering relies on the simulated transport history only and not on the in-situ observations, it is remarkable that the clustering excellently separates the episode of elevated levels from periods with low PAN. This in itself already indicates that large parts of the PAN variability actually depend on the transport history and may be explained by analysing the conditions during the different transport regimes in detail.

In the following, the observed time series are further interpreted following the obtained transport clustering. The results of the latter are displayed in Figs. 4 and 5 as cluster average surface SRRs and cluster average latitude-altitude SRR distributions for the European domain, respectively. Similar Figures for the larger North Atlantic region can be found in the Supplement (Figs. S1 and S2). In addition to the observed trace gas time series, the observations were split by transport cluster and aggregated to average diurnal cycles (Figs. 6 and 7). Where available, parameters from the less elevated sites, usually residing in the PBL or night-time residual layer, were treated in the same way, using the clustering as obtained for the nearby high Alpine site. For JFJ the average from the Swiss PBL sites (CHA and RIG) was taken, while for ZSF the observations from HPB were used as PBL reference. Observed PAN–CO relationships at the high Alpine sites, again disaggregated by transport cluster, are depicted in Fig. 8. Regression slopes were calculated from 3 hourly data using weighted total least square regression (Krystek and Anton, 2007), which takes the measurement uncertainty of both variables into account.

In a simplified way correlations between CO and PAN can be understood as follows. Assuming a constant PAN and CO background, emissions will lead to an initial increase in CO and PAN precursors in an air mass. During transport from the source to the receptor PAN may be produced under favourable conditions while CO can be assumed to remain relatively constant. During transport the original pollution “plume” will further mix with background air masses. The interception of different degrees of mixed air masses at the receptor will then result in correlation between CO and PAN spanning the range between the two endpoints of background conditions and pollution plume. The stronger the correlation the closer this simplified view actually matches reality, while weak correlations may indicate both: minor PAN production and/or ill-defined pollution plumes. The steeper the regression the more efficient PAN was produced in the original plume.

Finally and to foster the interpretation in terms of vertical mixing and local photochemical production, cluster average afternoon (12:00 and 15:00 UTC) PBL heights and daytime (06:00, 09:00, 12:00, and 15:00 UTC) cloud cover maps for Central Europe were derived from ECMWF-IFS operational analysis and forecast data, the same as used for the transport simulations (Fig. 9). PBL heights were derived by applying a critical Richardson number criterion (Vogelezang and Holtslag, 1996).

The individual transport clusters can be described as follows:

Cluster 1 (westerly advection). The SRRs in this cluster indicate a cyclonic flow from the North Atlantic region passing over the Iberian Peninsula and France before reaching JFJ and ZSF (Figs. 4 and 5 and Supplement S1 and S2). Additional influence from the western Mediterranean was identified for ZSF. While in general westerly advection with descending flow dominated this cluster, mainly representing air masses from lower tropospheric levels, sampled air masses had occasional PBL contact over France, Switzerland and, in the case of ZSF, southern Germany (Fig. 4, right panel). The influence of surface emissions was larger for ZSF than JFJ, as indicated by greater SRRs for the first. This category was experienced during an uninterrupted period from the beginning of May to 5 May. PAN concentrations were relatively low, in the range between 0.2–0.5 ppb at ZSF but dropped below this range at JFJ from 3 May onwards. This coincides with a period of decreased CO and O_3 at JFJ (see above). From the presented continental scale SRRs the difference in transport patterns between JFJ and ZSF is not apparent. However, when looking at the SRRs for the larger Northern Hemisphere (see Figs. S1 and S2) it becomes clear that in the case of JFJ parts of the air masses summarized in this transport regime actually originated over the southern North Atlantic, were transported northward over the Atlantic and finally advected towards Europe. This partially tropical origin could explain the relatively low mole fractions of CO and O_3 as observed at JFJ during the second half of this transport regime. Similar transport events towards JFJ were previously reported by (Bond et al., 2011), who documented the influence of advection from low northern latitudes on molecular hydrogen, methane and CO. Primary pollutant concentrations in this cluster were generally low. Occasionally high O_3 mixing ratios may indicate the influence of higher altitude air masses. At both sites, no pronounced diurnal cycle was observed for PAN, NO_y or NO_x, while a weak afternoon increase in CO and specific humidity could be seen for JFJ. NO_x, CO and specific humidity differences between the PBL and the high Alpine sites were larger for JFJ suggesting a larger degree of decoupling of the site from the PBL as in the case of ZSF (Figs. 6 and 7). According to model derived average afternoon PBL heights both sites were influenced by PBL air in the afternoon (Fig. 9). Cloud cover was rather large in the region that air masses passed prior to arrival at JFJ, indicating moderate photochemical turnover in these air masses. For ZSF air masses had a less direct transport path from the west and showed surface contact also in regions that were more cloud free (south-western Germany, south-western France). These observations also agree with the estimated regression slopes of PAN to CO that were steeper for ZSF than JFJ indicating less efficient PAN production in the air mass that reached JFJ. Overall the PAN/CO slope exhibited moderate values in this cluster. In summary, the observed conditions were not favourable of regional scale PAN production from recent emissions for JFJ, but indicated recent production for ZSF due to increased emission contact of the sampled air masses.

Cluster 2 (recirculating north-easterly/south-westerly advection). This flow regime comprises air masses that mainly arrived from north-easterly directions with additional surface influence south-west of the sites (Figs. 4 and 5). This is not the consequence of overlaying two separate transport regimes at different times, but is also characteristic for most of the individual SSRs during this period. The core of the backward plume typically moved slowly south-westward before taking a north-easterly and ascending path. Finally, part of the plume was recirculated westwards at higher altitudes and detrained into the PBL again, causing increased surface emission sensitivities west of the sites. The surface footprint for JFJ in the Fig. 4 indicates relatively large emission sensitivities over the western Alps and France, the easterly component is more pronounced for ZSF with strong sensitivities along the northern flank of the Alps in Austria and Bavaria. The regime occurred on 5 and 6 May and again between 18 and 25 May. This cluster showed considerable PBL contact in agreement with high water vapour content as observed at the sites. PAN mole fractions at both sites remained moderate for most of the category (∼ 0.4 and 0.3 ppb for JFJ and ZSF, respectively). However, JFJ experienced a few hours of high PAN on 6 May which fell into this cluster and caused the late afternoon peak in the overall diurnal cycle for this cluster (Fig. 6). Average daytime cloud cover was relatively large in this category (Fig. 9) suggesting weak photochemical activity and, hence, little potential for regional scale photochemical production of PAN from recent emissions. This is also supported by the insignificant correlations between PAN and CO as observed at ZSF and the relatively small PAN/CO slope at JFJ (Fig. 8). Again, the large PAN/CO correlation at JFJ results from the measurements on 6 May that were not typical for this cluster. Furthermore, it was mentioned earlier that trace gas observations on 23 May at JFJ suggested a short phase of stratospheric influence (high O_3, low CO and humidity). This is supported by the dispersion calculation that indicates air originating from the tropopause region over north-western France (see Fig. S3).

Cluster 3 (easterly advection). The SRRs in this cluster describe typical anti-cyclonic conditions with easterly to north-easterly advection and descending air masses. In addition, a southerly component close to the sites caused enhanced surface emission sensitivities in northern Italy and Switzerland for JFJ and Austria and to a smaller degree northern Italy for ZSF (Fig. 4). From Fig. 5 it can be seen that during this period free tropospheric air masses descended in the anticyclone. However, air masses had contact with the PBL shortly before reaching the sites, as can be seen by the relatively focused surface SRRs (Fig. 4). By far the highest pollutant concentrations were observed in this cluster including maxima for PAN, NO_y, NO_z, O_3 and CO. The descending air flow in this category may suggest that the observed PAN was mainly of free-tropospheric origin. However, the following considerations against this hypothesis can be made. First, next to PAN also CO was elevated at both sites. While part of this CO may have been produced in free-troposphere from VOC and CH_4 degradation, it seems more likely that it stems from direct surface emissions. Second, the decreased cloud cover over southern Germany and Eastern Europe favoured PBL photochemical production of PAN from fresh emissions in the PBL. Third, PAN levels at ZSF were as high as at the nearby PBL site HPB (Fig. 6). No diurnal cycle of PAN was observed at ZSF and the model estimated daytime PBL top was well above the sites altitude (Fig. 9). Both suggesting that ZSF was completely within the daytime PBL and remained within a residual layer during the night. This is in contrast to the usually intermittent PBL influence observed at high altitude sites, caused by the injection of PBL air into the FT over Alpine terrain (Henne et al., 2004; De Wekker et al., 2004). If ZSF was completely situated within the PBL or residual layer it is more likely that PAN was recently produced from fresh emission than from increases in hemispheric background levels. Fourth, PAN was larger at JFJ as compared to ZSF and showed a diurnal cycle typical of day-time injections of PBL air (see Fig. 6). This is also supported by a similar diurnal cycle in CO and specific humidity. No systematic diurnal cycle was observed for O_3 at JFJ, most probably due to the fact that afternoon PBL O_3 mole fractions were similar in the PBL as indicated by the observations at CHA and RIG (where night-time values were decreased due to surface deposition) see Fig. 6. PAN production in such PBL injections can be very efficient since large amounts of fresh precursors (NO_x and peroxyacyl radicals) are available and the air mass is adiabatically cooled during the injection, moving the NO_2-PAN balance towards PAN (Henne et al., 2005). The average

PAN/CO slope at JFJ was 0.023 as compared with 0.016 at ZSF (Fig. 8), suggesting that additional, rapid PAN production took place when PBL air was injected into the lower FT. The relatively small correlation coefficient at JFJ (0.56) as compared to ZSF (0.75) may indicate various levels of PAN production efficiencies in different PBL injections. At night-time PAN levels at JFJ were comparable to those at ZSF or even fell under those at ZSF (8 and 9 May, Fig. 3). NO_y levels were comparable for both sites. However, the PAN/NO_y ratio was larger at JFJ, which again indicates fresh PAN production, since no precipitation occurred in this regime, which could have washed out NO_y. Precursor levels in the PBL adjacent to JFJ were actually larger (NO_x 3–5 ppb) as compared with HPB (< 2 ppb). For JFJ large emission sensitivities over the western Po Valley were estimated. The western Po Valley including the metropolitan area of Milan comprises large anthropogenic emissions of NO_x and VOCs (e.g. Prevot et al., 1997) and weak ventilation conditions favour the accumulation of pollutants. In addition, large amounts of biogenic VOC emissions occur within the Alpine region and may deliver the amount of peroxyacyl radicals required for strong PAN production.

In summary, these observations point towards a regional scale production of PAN in the PBL, which may further be enhanced when PBL air masses are lifted into the lower FT, where they were sampled at JFJ.

Cluster 4 (south-easterly advection). Figure 4 shows that air masses combined in this cluster had only weak surface contact, mainly close to the sites within the Alps and over Italy and the adjacent parts of the Mediterranean. The respective air masses remained within the lower FT north of 30° N prior to arrival at the sites (see Figs. S1 and S2 in the Supplement). This flow pattern occurred during two episodes in May 2008, namely 15–18 May and 26–31 May. For ZSF two transport clusters were present during these periods, the second one is described below. The current cluster showed low PAN mean concentrations of 0.2–0.4 ppb and also experienced rather low other trace gas concentrations (NO_x, NO_y, CO). No diurnal cycle in any of the trace species was observed at either site, compared to close by PBL sites in Fig. 6. Hence, the influence from recent emissions on these air masses was considered small. Recent photochemical processing in these air masses was probably low due to relatively large cloud cover over the Alps and Northern Italy. The PAN/CO slope at JFJ was the largest compared to all other transport regimes. However, this was mainly caused by the attribution of high PAN levels on 15 May to this cluster. This day was the last of the high PAN episode and probably better related to cluster 3 than to this transport cluster. Without the data from 15 May correlation coefficient and slope considerably decreased. Similar arguments can be made for ZSF, where PAN mixing ratios were still large on 15 and 16 May, which were assigned to the current cluster, but probably should have been assigned to the high PAN cluster (3).

Cluster 5 (southerly advection, ZSF only). This SRR describes the transport path from the South, with moderate SRRs over the Mediterranean and Italy and additional boundary layer contact in the Alpine region. In line with the transport simulations, PAN, NO_y, and CO mixing ratios were the lowest in this cluster. Due to the southern, low tropospheric origin of the air masses, these were relatively warm and moist as compared to the other transport clusters. While the correlation between PAN and CO was the strongest of all clusters, the regression slope was the smallest, indicating inefficient PAN production, most likely due to the lack of available NO_2.

5 Conclusions

In agreement with previous studies PAN measurements from ZSF and JFJ showed a pronounced seasonal cycle with maximum mole fractions in late spring. This indicates that the spring maximum of PAN in background air masses as observed at other northern hemispheric sites is also a typical phenomenon at high Alpine sites. The origin of the spring-time maximum was evaluated in more detail for May 2008 when PAN levels were especially large. Different transport regimes towards the sites were distinguished using a clustering method on backward dispersion simulations. These show that air masses in May 2008 had recent PBL contact in different parts of Europe before reaching the measurement stations at JFJ and ZSF. At both sites, the highest

PAN concentrations of May 2008 were connected with descending air masses in anti-cyclonic flow (cluster 3). However, these air masses experienced pronounced contact with the PBL under photo-chemically favourable (cloud free) conditions, prior to the arrival at the sites. Comparison with nearby PBL sites reveal that the ZSF observatory was situated within the day-time PBL, while JFJ was influenced by PBL injections during this period. PAN levels were considerably lower during all other flow regimes also for those less influenced by recent PBL contact. From the three hypothesis formulated in the introduction, our results show that the PAN spring maximum in the lower FT over Europe, as sampled at two high Alpine sites, is mainly caused by the following factors: (1) high pressure conditions lead to an accumulation of trace gases in the PBL and vertical transport from the PBL becomes important for transporting the pollutants to the sites (2) solar irradiance is already large in May which enhances the photochemistry during cloud free conditions as encountered during the anti-cyclonic transport regime (3) temperatures are still relatively low in the lower free troposphere preventing thermal decomposition of PAN which becomes more important in summer.

The analysis of the high spring PAN mixing ratios at these Alpine sites clearly suggests that the spring maximum is primarily caused by PAN production in and export from the regional PBL. An additional, but smaller, spring-time increase in the hemispheric PAN background cannot be ruled out from the current analysis. However, highest PAN observations during May 2008 were not connected with free tropospheric conditions, but with PBL air masses. These results agree well with those of Pandey Deolal et al. (2013) that, based on hemispheric scale backward trajectories, indicate that those air masses which had surface contact in the European boundary layer were associated with largest PAN and NO_y mixing ratios in spring and are attributable to European boundary layer sources and not inter-continental transport or free tropospheric production. Observed PAN differences between the sites were not directly linked to temperature differences, suggesting that thermal decomposition cannot be solely responsible for these differences, but that local to regional scale production/destruction plays an important role.

The Supplement related to this article is available online at doi:10.5194/acpd-14-12727-2014-supplement.

Acknowledgements. We thank the Swiss National Foundation (SNF) for providing funding of projects Nr. 200020-117626 and 206021_128754 to carry out this research. We also express our gratitude towards international foundation for high-alpine research stations Jungfraujoch and Gornergrat (HFSJG) for providing access to Jungfraujoch facilities and respective custodians for their support. We are thankful to NABEL for their data, which is operated by Empa in collaboration with the Swiss Federal Office for the Environment. We also thank MeteoSwiss for provision of meteorological data from Jungfraujoch.

References

Balzani Lööv, J. M., Henne, S., Legreid, G., Staehelin, J., Reimann, S., Prevot, A. S. H., Steinbacher, M., and Vollmer, M. K.: Estimation of background concentrations of trace gases at the Swiss Alpine site Jungfraujoch (3580 m a.s.l.), J. Geophys. Res., 113, D22305, doi:10.1029/2007JD009751, 2008.

Bond, S. W., Vollmer, M. K., Steinbacher, M., Henne, S., and Reimann, S.: Atmospheric molecular hydrogen (H-2): observations at the high-altitude site Jungfraujoch, Switzerland, Tellus B, 63, 64–76, doi:10.1111/j.1600-0889.2010.00509.x, 2011.

Bottenheim, J. W., Sirois, A., Brice, K. A., and Gallant, A. J.: Five years of continuous observations of PAN and ozone at a rural location in eastern Canada, J. Geophys. Res., 99, 5333–5352, doi:10.1029/93JD02716, 1994.

Brunner, D., Henne, S., Keller, C. A., Reimann, S., Vollmer, M. K., O'Doherty, S., and Maione, M.: An extended Kalman-filter for regional scale inverse emission estimation, Atmos. Chem. Phys., 12, 3455–3478, doi:10.5194/acp-12-3455-2012, 2012.

Cooper, O. R., Parrish, D. D., Stohl, A., Trainer, M., Nedelec, P., Thouret, V., Cammas, J. P., Oltmans, S. J., Johnson, B. J., Tarasick, D., Leblanc, T., McDermid, I. S., Jaffe, D., Gao, R., Stith, J., Ryerson, T., Aikin, K., Campos, T., Weinheimer, A., and Avery, M. A.: Increasing springtime ozone mixing ratios in the free troposphere over western North America, Nature, 463, 344–348, doi:10.1038/nature08708, 2010.

De Wekker, S. F. J., Steyn, D. G., and Nyeki, S.: A comparison of aerosol layer- and convective boundary layer structure over a mountain range during STAAARTE '97, Bound.-Lay. Meteorol., 113, 249–271, 2004.

Empa and FOEN: Technischer Bericht zum Nationalen Beobachtungsnetz für Luftfremdstoffe (NABEL) 2013, Empa, Duebendorf, Switzerland, available at: http://www.empa.ch/plugin/template/empa/*/139851 (last access: 9 May 2014), 226, 2013.

Fenneteaux, I., Colin, P., Etienne, A., Boudries, H., Dutot, A. L., Perros, P. E., and Toupance, G.: Influence of continental sources on oceanic air composition at the eastern edge of the North Atlantic Ocean, TOR 1992–1995, J. Atmos. Chem., 32, 233–280, doi:10.1023/A:1006140223711, 1999.

Fiore, A. M., Dentener, F. J., Wild, O., Cuvelier, C., Schultz, M. G., Hess, P., Textor, C., Schulz, M., Doherty, R. M., Horowitz, L. W., MacKenzie, I. A., Sanderson, M. G., Shindell, D. T., Stevenson, D. S., Szopa, S., Van Dingenen, R., Zeng, G., Atherton, C., Bergmann, D., Bey, I., Carmichael, G., Collins, W. J., Duncan, B. N., Faluvegi, G., Folberth, G., Gauss, M., Gong, S., Hauglustaine, D., Holloway, T., Isaksen, I. S. A., Jacob, D. J., Jonson, J. E., Kaminski, J. W., Keating, T. J., Lupu, A., Marmer, E., Montanaro, V., Park, R. J., Pitari, G., Pringle, K. J., Pyle, J. A., Schroeder, S., Vivanco, M. G., Wind, P., Wojcik, G., Wu, S., and Zuber, A.: Multimodel estimates of intercontinental source–receptor relationships for ozone pollution, J. Geophys. Res., 114, D04301, doi:10.1029/2008JD010816, 2009.

Fischer, E. V., Jaffe, D. A., Reidmiller, D. R., and Jaeglé, L.: Meteorological controls on observed peroxyacetyl nitrate at Mount Bachelor during the spring of 2008, J. Geophys. Res., 115, D03302, doi:10.1029/2009JD012776, 2010.

Gantner, L., Hornsteiner, M., Egger, J., and Hartjenstein, G.: The diurnal circulation of Zugspitzplatt: observations and modeling, Meteorol. Z., 12, 95–102, doi:10.1127/0941-2948/2003/0012-0095, 2003.

Gilge, S., Plass-Duelmer, C., Fricke, W., Kaiser, A., Ries, L., Buchmann, B., and Steinbacher, M.: Ozone, carbon monoxide and nitrogen oxides time series at four alpine GAW mountain stations in central Europe, Atmos. Chem. Phys., 10, 12295–12316, doi:10.5194/acp-10-12295-2010, 2010.

Hamburger, T., McMeeking, G., Minikin, A., Birmili, W., Dall'Osto, M., O'Dowd, C., Flentje, H., Henzing, B., Junninen, H., Kristensson, A., de Leeuw, G., Stohl, A., Burkhart, J. F., Coe, H., Krejci, R., and Petzold, A.: Overview of the synoptic and pollution situation over Europe during the EUCAARI-LONGREX field campaign, Atmos. Chem. Phys., 11, 1065–1082, doi:10.5194/acp-11-1065-2011, 2011.

Henne, S., Furger, M., Nyeki, S., Steinbacher, M., Neininger, B., de Wekker, S. F. J., Dommen, J., Spichtinger, N., Stohl, A., and Prévôt, A. S. H.: Quantification of topographic venting of boundary layer air to the free troposphere, Atmos. Chem. Phys., 4, 497–509, doi:10.5194/acp-4-497-2004, 2004.

Henne, S., Dommen, J., Neininger, B., Reimann, S., Staehelin, J., and Prevot, A. S. H.: Influence of mountain venting in the Alps on the ozone chemistry of the lower free troposphere and the European pollution export, J. Geophys. Res., 110, D22307, 2005.

Henne, S., Brunner, D., Folini, D., Solberg, S., Klausen, J., and Buchmann, B.: Assessment of parameters describing representativeness of air quality in-situ measurement sites, Atmos. Chem. Phys., 10, 3561–3581, doi:10.5194/acp-10-3561-2010, 2010.

Hirdman, D., Sodemann, H., Eckhardt, S., Burkhart, J. F., Jefferson, A., Mefford, T., Quinn, P. K., Sharma, S., Ström, J., and Stohl, A.: Source identification of short-lived air pollutants in the Arctic using statistical analysis of measurement data and particle dispersion model output, Atmos. Chem. Phys., 10, 669–693, doi:10.5194/acp-10-669-2010, 2010.

Kaiser, A., Scheifinger, H., Spangl, W., Weiss, A., Gilge, S., Fricke, W., Ries, L., Cemas, D., and Jesenovec, B.: Transport of nitrogen oxides, carbon monoxide and ozone to the Alpine Global Atmosphere Watch stations Jungfraujoch (Switzerland), Zugspitze and Hohenpeissenberg (Germany), Sonnblick (Austria) and Mt. Krvavec (Slovenia), Atmos. Environ., 41, 9273–9287, doi:10.1016/j.atmosenv.2007.09.027, 2007.

Kaufman, L. and Rousseeuw, P. J.: Finding Groups in Data, an Introduction to Cluster Analysis, John Wiley and Sons, New York, 342 pp., 1990.

Keller, C. A., Brunner, D., Henne, S., Vollmer, M. K., O'Doherty, S., and Reimann, S.: Evidence for under-reported western European emissions of the potent greenhouse gas HFC-23, Geophys. Res. Lett., 38, L15808, doi:10.1029/2011GL047976, 2011.

Keller, C. A., Hill, M., Vollmer, M. K., Henne, S., Brunner, D., Reimann, S., O'Doherty, S., Arduini, J., Maione, M., Ferenczi, Z., Haszpra, L., Manning, A. J., and Peter, T.: European emissions of halogenated greenhouse gases inferred from atmospheric measurements, Environ. Sci. Technol., 46, 217–225, doi:10.1021/es202453j, 2012.

Krystek, M. and Anton, M.: A weighted total least-squares algorithm for fitting a straight line, Meas. Sci. Technol., 18, 3438–3442, 2007.

Monks, P. S.: A review of the observations and origins of the spring ozone maximum, Atmos. Environ., 34, 3545–3561, 2000.

Moxim, W. J., Levy, H., and Kasibhatla, P. S.: Simulated global tropospheric PAN: its transport and impact on NO_x, J. Geophys. Res., 101, 12621–12638, 1996.

Nielsen, T., Samuelsson, U., Grennfelt, P., and Thomsen, E. L.: Peroxyacetyl nitrate in long-range transported polluted air, Nature, 293, 553–555, 1981.

Ordóñez, C., Elguindi, N., Stein, O., Huijnen, V., Flemming, J., Inness, A., Flentje, H., Katragkou, E., Moinat, P., Peuch, V.-H., Segers, A., Thouret, V., Athier, G., van Weele, M., Zerefos, C. S., Cammas, J.-P., and Schultz, M. G.: Global model simulations of air pollution during the 2003 European heat wave, Atmos. Chem. Phys., 10, 789–815, doi:10.5194/acp-10-789-2010, 2010.

Pandey Deolal, S., Brunner, D., Steinbacher, M., Weers, U., and Staehelin, J.: Long-term in situ measurements of NO_x and NO_y at Jungfraujoch 1998–2009: time series analysis and evaluation, Atmos. Chem. Phys., 12, 2551–2566, doi:10.5194/acp-12-2551-2012, 2012.

Pandey Deolal, S., Staehelin, J., Brunner, D., Cui, J., Steinbacher, M., Zellweger, C., Henne, S., and Vollmer, M. K.: Transport of PAN and NO_y from different source regions to the Swiss high alpine site Jungfraujoch, Atmos. Environ., 64, 103–115, doi:10.1016/j.atmosenv.2012.08.021, 2013.

Parker, A. E., Monks, P. S., Wyche, K. P., Balzani-Lööv, J. M., Staehelin, J., Reimann, S., Legreid, G., Vollmer, M. K., and Steinbacher, M.: Peroxy radicals in the summer free troposphere: seasonality and potential for heterogeneous loss, Atmos. Chem. Phys., 9, 1989–2006, doi:10.5194/acp-9-1989-2009, 2009.

Penkett, S. A. and Brice, K. A.: The spring maximum in photooxidants in the Northern Hemisphere Troposphere, Nature, 319, 655–657, 1986.

Penkett, S. A., Blake, N. J., Lightman, P., Marsh, A. R. W., Anwyl, P., and Butcher, G.: The seasonal variation of nonmethane hydrocarbons in the free troposphere over the North Atlantic Ocean: possible evidence for extensive reaction of hydrocarbons with the nitrate radical, J. Geophys. Res., 98, 2865–2885, doi:10.1029/92JD02162, 1993.

Prevot, A. S. H., Staehelin, J., Kok, G. L., Schillawski, R. D., Neininger, B., Staffelbach, T., Neftel, A., Wernli, H., and Dommen, J.: The Milan photooxidant plume, J. Geophys. Res., 102, 23375–23388, 1997.

Rappenglück, B., Dasgupta, P. K., Leuchner, M., Li, Q., and Luke, W.: Formaldehyde and its relation to CO, PAN, and SO_2 in the Houston-Galveston airshed, Atmos. Chem. Phys., 10, 2413–2424, doi:10.5194/acp-10-2413-2010, 2010.

Reiter, R., Sladkovic, R., and Kanter, H. J.: Concentration of trace gases in the lower troposphere, simultaneously recorded at neighboring mountain stations, Part II: Ozone, Meteorol. Atmos. Phys., 37, 27–47, doi:10.1007/BF01047008, 1987.

Ridley, B., Walega, J., Hübler, G., Montzka, D., Atlas, E., Hauglustaine, D., Grahek, F., Lind, J., Campos, T., Norton, R., Greenberg, J., Schauffler, S., Oltmans, S., and Whittlestone, S.: Measurements of NO_x and PAN and estimates of O_3 production over the seasons during Mauna Loa Observatory Photochemistry Experiment 2, J. Geophys. Res., 103, 8323–8339, doi:10.1029/98JD00075, 1998.

Schrimpf, W., Linaerts, K., Müller, K. P., Koppmann, R., and Rudolph, J.: Peroxyacetyl nitrate (PAN) measurements during the POPCORN Campaign, J. Atmos. Chem., 31, 139–159, doi:10.1023/A:1006004031055, 1998.

Seibert, P. and Frank, A.: Source-receptor matrix calculation with a Lagrangian particle dispersion model in backward mode, Atmos. Chem. Phys., 4, 51–63, doi:10.5194/acp-4-51-2004, 2004.

Stohl, A., Forster, C., Frank, A., Seibert, P., and Wotawa, G.: Technical note: The Lagrangian particle dispersion model FLEXPART version 6.2, Atmos. Chem. Phys., 5, 2461–2474, doi:10.5194/acp-5-2461-2005, 2005.

Sturm, P., Tuzson, B., Henne, S., and Emmenegger, L.: Tracking isotopic signatures of CO_2 at the high altitude site Jungfraujoch with laser spectroscopy: analytical improvements and representative results, Atmos. Meas. Tech., 6, 1659–1671, doi:10.5194/amt-6-1659-2013, 2013.

Tsalkani, N., Perros, P., Dutot, A. L., and Toupance, G.: One-year measurements of PAN in the Paris basin: effect of meteorological parameters, Atmos. Environ., 25, 1941–1949, doi:10.1016/0960-1686(91)90275-C, 1991.

Tyndall, G. S., Apel, E., Williams, E., Flocke, F., Cohen, R. C., Gilge, S., Kim, S., Mills, G., O'Brien, J., Perring, A., Rappenglueck, B., Roberts, J., Schmitt, R., Swanson, A., Tanimoto, H., and Wooldridge, P. J.: PIE 2005: An intercomparison of measurement techniques for peroxynitrates (PANs), AGU Fall Meeting, 5–9 December 2005, San Francisco, CA, USA, Abstract A13C-0941, 2005.

Vogelezang, D. H. P. and Holtslag, A. A. M.: Evaluation and model impacts of alternative boundary-layer height formulations, Bound.-Lay. Meteorol., 81, 245–269, 1996.

Vollmer, M. K., Zhou, L., Greally, B. R., Henne, S., Yao, B., Reimann, S., Stordal, F., Cunnold, D. M., Zhang, X., Maione, M., Zhang, F., Huang, J., and Simmonds, P. G.: Emissions of ozone-depleting halocarbons from China, Geophys. Res. Lett., 36, L15823, doi:10.1029/2009GL038659, 2009.

Whalley, L. K., Lewis, A. C., McQuaid, J. B., Purvis, R. M., Lee, J. D., Stemmler, K., Zellweger, C., and Ridgeon, P.: Two high-speed, portable GC systems designed for the measurement of non-methane hydrocarbons and PAN: results from the Jungfraujoch High Altitude Observatory, J. Environ. Monitor., 6, 234–241, 2004.

Wunderli, S. and Gehrig, R.: Influence of temperature of formation and stability of surface PAN and ozone, a two year field study in Switzerland, Atmos. Environ. A-Gen., 25, 1599–1608, doi:10.1016/0960-1686(91)90018-3, 1991.

Zanis, P., Monks, P. S., Green, T. J., Schuepbach, E., Carpenter, L. J., Mills, G. P., Rickard, A. R., Brough, N., and Penkett, S. A.: Seasonal variation of peroxy radicals in the lower free troposphere based on observations from the FREE Tropospheric EXperiments in the Swiss Alps, Geophys. Res. Lett., 30, 1497, doi:10.1029/2003GL017122, 2003.

Zanis, P., Ganser, A., Zellweger, C., Henne, S., Steinbacher, M., and Staehelin, J.: Seasonal variability of measured ozone production efficiencies in the lower free troposphere of Central Europe, Atmos. Chem. Phys., 7, 223–236, doi:10.5194/acp-7-223-2007, 2007.

Zellweger, C., Ammann, M., Buchmann, B., Hofer, P., Lugauer, M., Ruttimann, R., Streit, N., Weingartner, E., and Baltensperger, U.: Summertime NO_y speciation at the Jungfraujoch, 3580 m a.s.l., Switzerland, J. Geophys. Res., 105, 6655–6667, 2000.

Zellweger, C., Forrer, J., Hofer, P., Nyeki, S., Schwarzenbach, B., Weingartner, E., Ammann, M., and Baltensperger, U.: Partitioning of reactive nitrogen (NO_y) and dependence on meteorological conditions in the lower free troposphere, Atmos. Chem. Phys., 3, 779–796, doi:10.5194/acp-3-779-2003, 2003.

Zellweger, C., Hüglin, C., Klausen, J., Steinbacher, M., Vollmer, M., and Buchmann, B.: Intercomparison of four different carbon monoxide measurement techniques and evaluation of the long-term carbon monoxide time series of Jungfraujoch, Atmos. Chem. Phys., 9, 3491–3503, doi:10.5194/acp-9-3491-2009, 2009.

Table 1. Characteristics of measurement sites: High Alpine sites (Jungfraujoch, JFJ and Zugspitze Schneefernerhaus, ZSF), which are intermittently within the free troposphere (FT) and influenced by boundary layer injections, and elevated rural sites (Hohenpeissenberg, HPB; Rigi, RIG; Chaumont, CHA), which are usually situated within the day-time planetary boundary layer but well above the night-time inversion layer. The given temperature and ambient pressure levels give the range of the observations in May 2008.

Parameter	Jungfraujoch (JFJ)	Zugspitze/Schneefernerhaus (ZSF)	Hohenpeissenberg (HPB)	Rigi (RIG)	Chaumont (CHA)
Country	Switzerland	Germany	Germany	Switzerland	Switzerland
Geographical coordinates	46.33° N 7.59° E	47.42° N 10.98° E	47.80° N 11.02° E	46.07° N 8.45° E	47.02° N 6.58° E
Altitude (m a.s.l.)	3580	2670	985	1031	1137
Temperature (K)	260–274	266–285	277–300	276–297	274–295
Pressure (hPa)	647–662	727–742	895–912	890–907	879–895
Category	High Alpine (FT/PBL)	High Alpine (FT/PBL)	Elevated rural (PBL)	Elevated rural (PBL)	Elevated rural (PBL)
Measurement operation (trace gases)	Empa	UBA	DWD	Empa	Empa

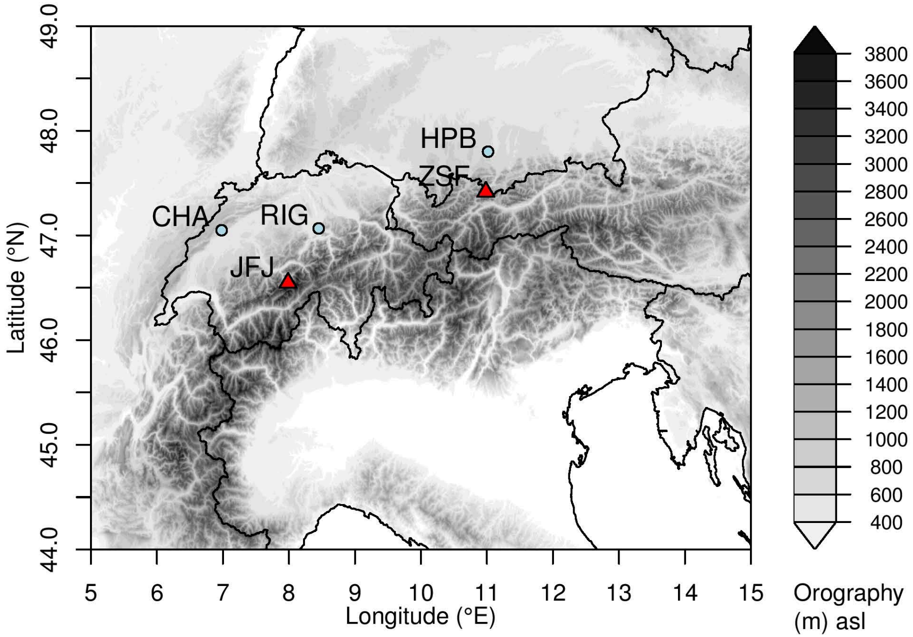

Figure 1. Red triangles: the locations of the two high Alpine stations Jungfraujoch (JFJ) and Zugspitze Schneefernerhaus (ZSF). Blue circles: the additional elevated PBL sites Chaumont (CHA), Rigi (RIG) and Hohenpeissenberg (HPB).

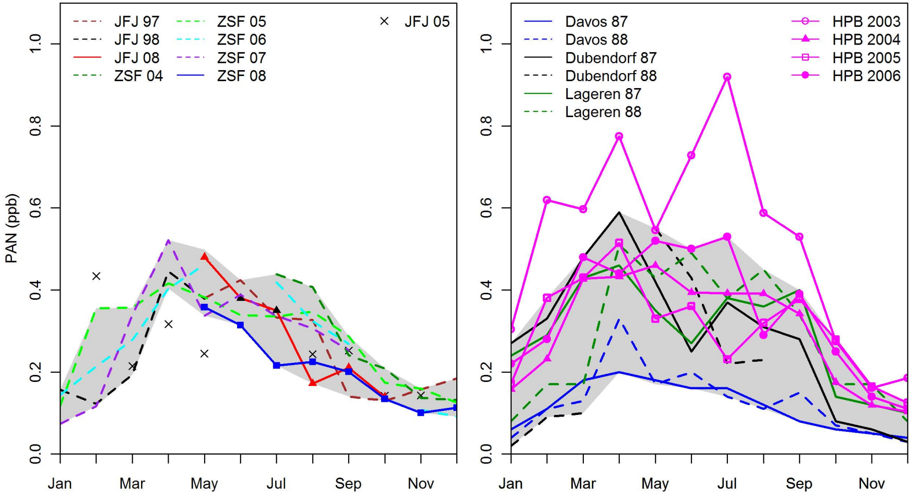

Figure 2. Left panel: monthly mean PAN mixing ratios at high mountain sites Jungfraujoch (JFJ) and Zugspitze Schneefernerhaus (ZSF). Black triangles: monthly mean values at JFJ from campaign 2008 dataset. Black crosses: campaign measurements at JFJ during February 2005–August 2006 from Balzani Lööv et al. (2008). The grey shaded area shows the measurement range of monthly averages based on continuous measurements of JFJ and ZSF. Right panel: PAN measurements of less elevated sites (Hohenpeissenberg, HPB) and PAN measurements during 1987–1988 from Wunderli and Gehrig (1991) for Swiss sub-urban (Dubendorf), rural (Lageren) and low level alpine site (Davos, 1630 m a.s.l.). The grey shaded area shows the measurement range based on all PAN measurements excluding 2003. * 2003 was marked as European heat wave.

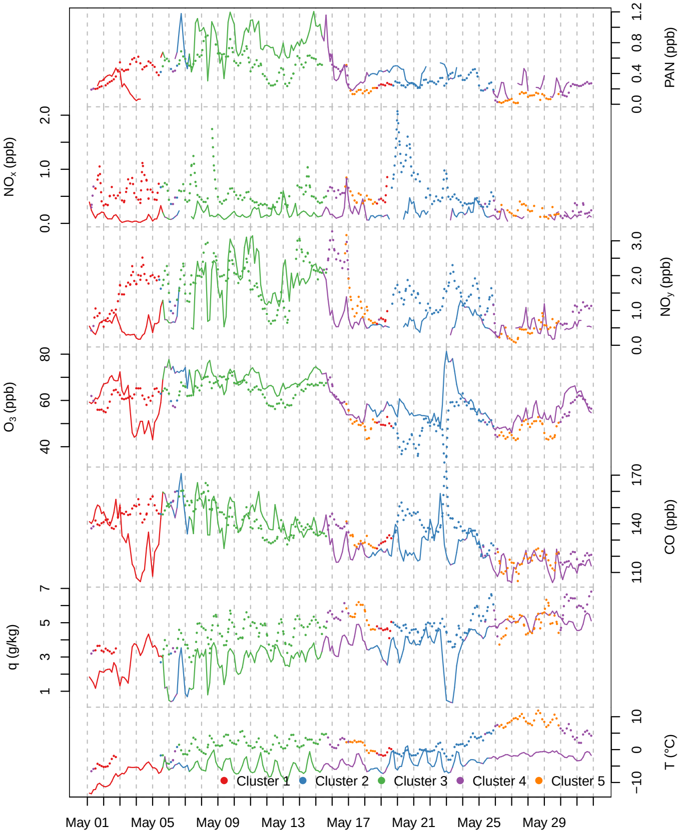

Figure 3. Observed 3 hourly averages of trace gas mixing ratios (ppbv), absolute humidity ($\mathrm{g\,kg^{-1}}$) and temperature (K) at (solid lines) Jungfraujoch and (dotted lines) Zugspitze in May 2008. The colour coding refers to the periods as identified by footprint clustering (see Sect. 4.2.3).

Title Page
Abstract | Introduction
Conclusions | References
Tables | Figures
◀| |▶
◀ ▶
Back | Close
Full Screen / Esc
Printer-friendly Version
Interactive Discussion

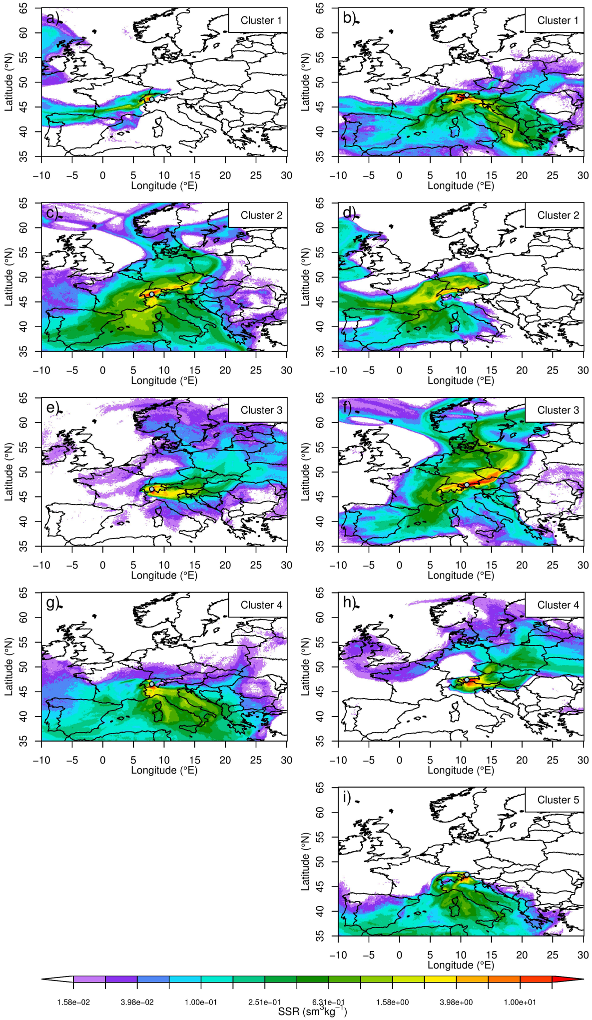
a)
Cluster 1
b)
Cluster 1
c)
Cluster 2
d)
Cluster 2
e)
Cluster 3
f)
Cluster 3
g)
Cluster 4
h)
Cluster 4
i)
Cluster 5
Latitude (°N)
35 40 45 50 55 60 65
Longitude (°E)
−10 −5 0 5 10 15 20 25 30
1.58e−02
3.98e−02
1.00e−01
2.51e−01
6.31e−01
1.58e+00
3.98e+00
1.00e+01
SSR (sm^{3}kg^{-1})

Figure 4. Cluster average surface SRRs for (left: **a, c, e, g**) JFJ and (right: **b, d, f, h, i**) ZSF. Larger SRR indicate a larger sensitivity of the samples air masses to surface fluxes (emissions or deposition). The sampling locations are given by a light blue circle.

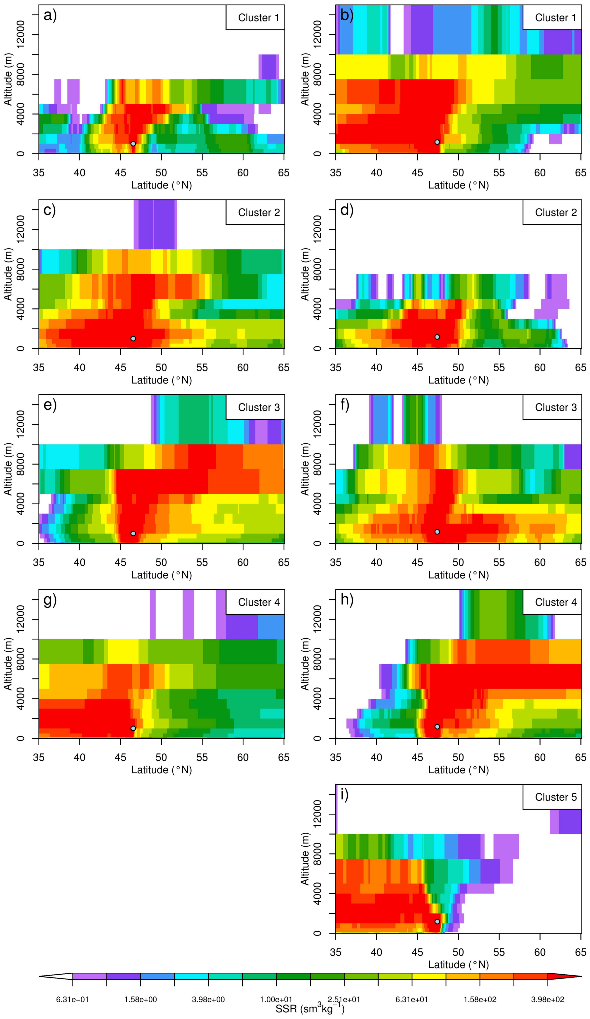

Title Page
Abstract | Introduction
Conclusions | References
Tables | Figures
◀I | ▶I
◀ | ▶
Back | Close
Full Screen / Esc
Printer-friendly Version
Interactive Discussion

Figure 5. Cluster average latitude-altitude distribution of SRRs for (left: **a, c, e, g**) JFJ and (right: **b, d, f, h, i**) ZSF. The sampling locations are given by a light blue circle.

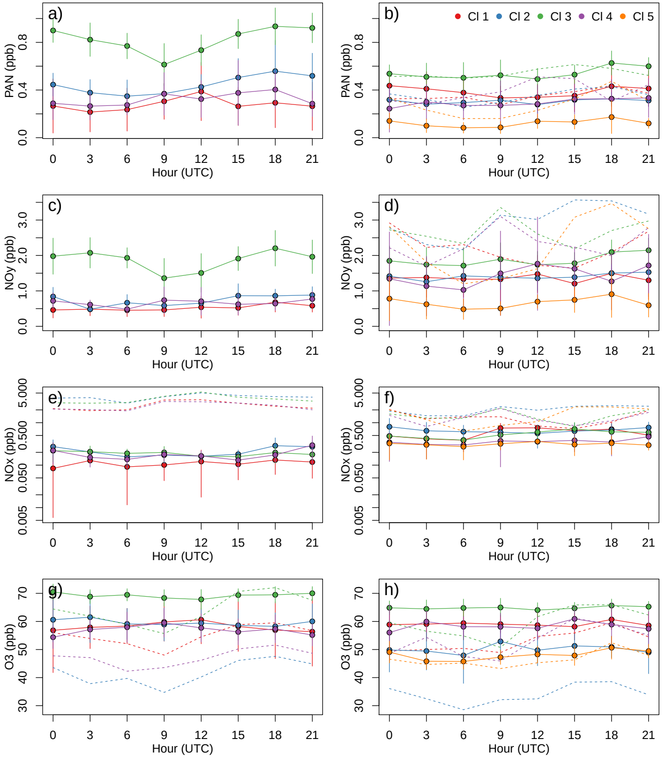

Figure 6. Average diurnal cycles of **(a, b)** PAN, **(c, d)** NO_y, **(e, f)** NO_x and **(g, h)** O_3 split by transport cluster as indicated by the different colours (see definition in **b**), which represent the same clusters as in Fig. 3. The solid lines and error bars represent the high Alpine measurements at (left: **a, c, e, g**) JFJ and (right: **b, d, f, h**) ZSF. The dotted lines give the average diurnal cycle as observed at the reference PBL sites: average of RIG and CHA for JFJ and HPB for ZSF. The error bars represent expanded uncertainty (95 % confidence limits) of the 3 hourly cluster means. Note that a logarithmic y-axis was chosen for NO_x. The time stamp of the 3 hourly aggregates corresponds to the end of the aggregation interval.

ACPD
14, 12727–12769, 2014

Title Page
Abstract | Introduction
Conclusions | References
Tables | Figures
◀| |▶
◀ ▶
Back | Close
Full Screen / Esc
Printer-friendly Version
Interactive Discussion

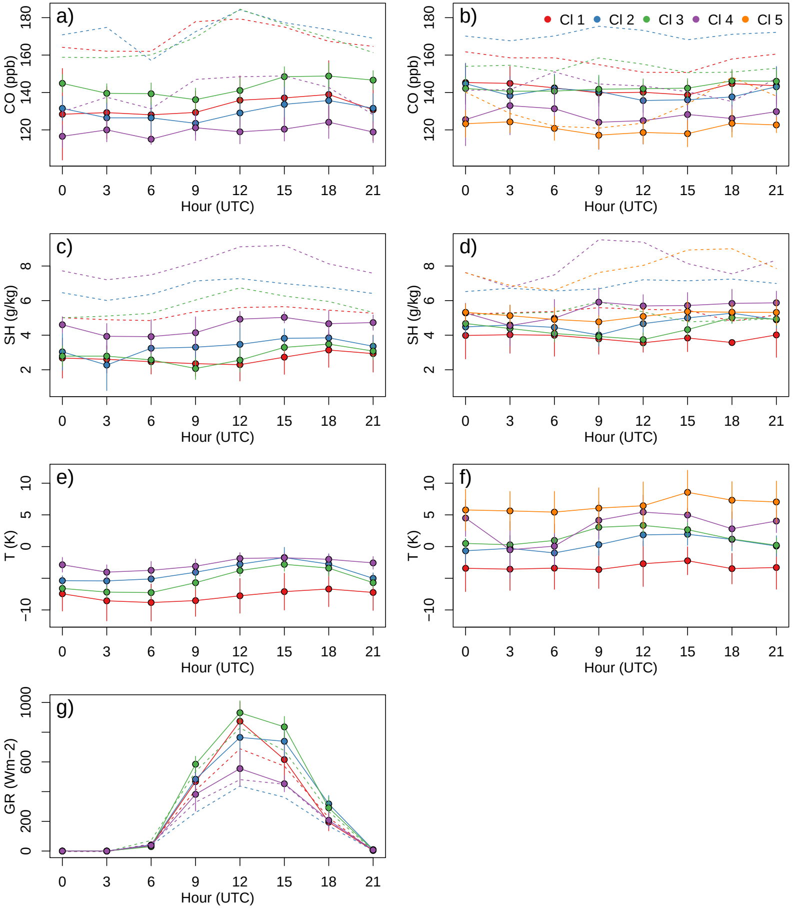

Figure 7. Same as Fig. 6, but for **(a, b)** CO, **(c, d)** specific humidity, **(e, f)** ambient temperature and **(g)** global radiation at (left: **a, c, e, g**) JFJ and (right: **b, d, f**) ZSF.

ACPD
14, 12727–12769, 2014

Title Page
Abstract Introduction
Conclusions References
Tables Figures
◀| |▶
◀ ▶
Back Close
Full Screen / Esc
Printer-friendly Version
Interactive Discussion

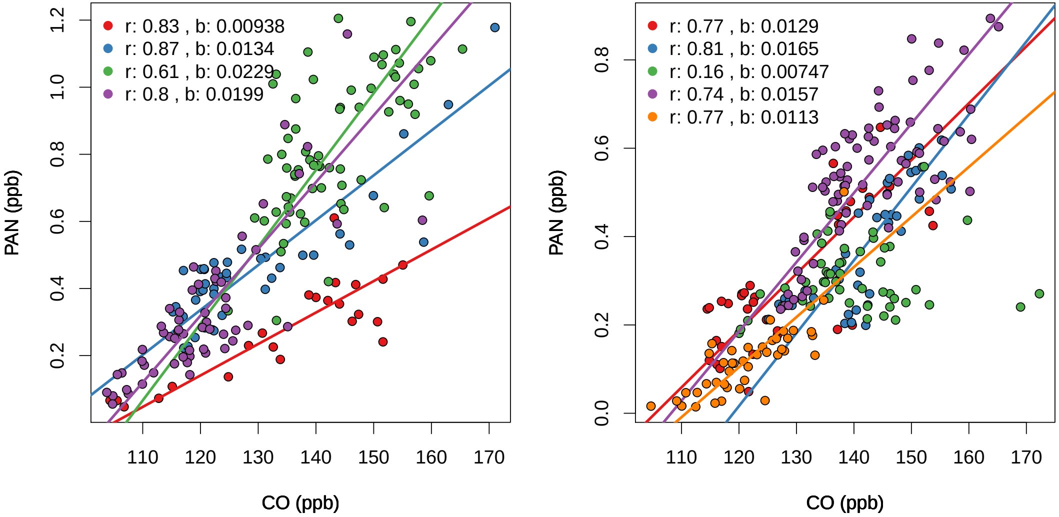

Figure 8. Scatter plots of observed PAN vs. CO mole fractions coloured by transport cluster for JFJ (left) and ZSF (right). Regression lines were obtained using weighted total least square regression. Regression lines are only shown if a significant correlation between PAN and CO was observed. (The colours represent the correlations within the individual transport clusters, see Fig. 3 and text.)

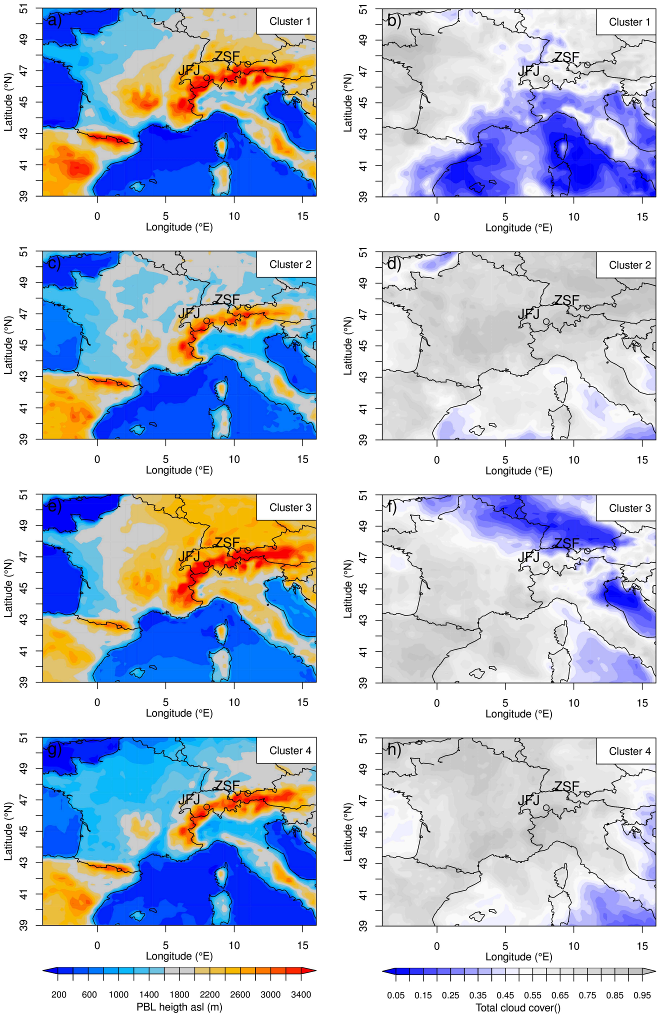

Title Page
Abstract
Introduction
Conclusions
References
Tables
Figures
◀I
▶I
◀
▶
Back
Close
Full Screen / Esc
Printer-friendly Version
Interactive Discussion

Figure 9. Cluster average for (left: **a, c, e, g**) afternoon PBL height and (right: **b, d, f, h**) daytime total cloud cover fraction for the transport clusters as derived for JFJ. Afternoon PBL heights were calculated from ECMWF-IFS operational analysis and forecast fields at 12:00 and 15:00 UTC using a critical Richardson number criterion. Day-time total cloud cover was taken from the same ECMWF fields at (06:00, 09:00, 12:00, and 15:00 UTC) UTC.